PNC SN9410 90-154

SELF-LIMITING MECHANISMS FOR CDA ENERGETICS BASED ON IN-PILE EXPERIMENT ANALYSIS AND IMPROVED REACTOR EVALUATION METHOD

October, 1990

O-ARAI ENGINEERING CENTER

POWER REACTOR AND NUCLEAR FUEL DEVELOPMENT CORPORATION

NOT FOR PUBLICATION
PNC SN9410 90-154
October, 1990

SELF-LIMITING MECHANISMS FOR CDA ENERGETICS BASED ON IN-PILE EXPERIMENT ANALYSIS AND IMPROVED REACTOR EVALUATION METHOD

N. NONAKA*
I. SATO*

ABSTRACT

The present report discusses the current understanding and improved evaluation method of key phenomena in the initiating-phase energetics of ULOF whole-core accidents in LMFBRs. Three phenomena, i.e. axial fuel expansion, fuel failure and post-failure fuel motion, have been examined through the CABRI-1 in-pile tests and analyses with special emphasis on the mechanisms for self-limiting the energetics potential.

Major important mechanisms, identified in this study, are: (1) fuel expansion effective to delay the ULOF-induced power burst; (2) fuel-dispersal potential activated under low energy condition in voided channels, and enhanced fuel mobility with increased heating rate; (3) above-midplane failure and failure extension effective particularly in partially voided channels.

The improved knowledge validated through the CABRI-1 analyses has been implemented to the revised SAS3D code as an improved evaluation method of CDAs, and the importance and effectiveness of the mechanisms were confirmed by the reactor application study.

KEYWORDS: initiating phase, energetics, self-limiting mechanism, ULOF accident, LOF-driven-TOP, in-pile tests, CABRI-1, coolant boiling, axial fuel expansion, burst fuel pin failure, fuel disruption, fuel motion, MFCI, reactivity feed-back, PAPAS-2S, SAS3D, SAS4A, CDA, LMFBR, safety

---

* FBR Safety Engineering Section, Safety Engineering Division,
O-arai Engineering Center

配　布　限　定
PNC SN9410 90-154
１９９０年１０月

炉内試験評価に基くＣＤＡエネルギー放出に対する自己制御機構の解明と実機評価手法の改善

野中信之*
佐藤一憲*

要　　旨

本報告は、高速炉の炉心崩壊事故（ＣＤＡ）に対する安全評価において重要となるＵＬＯＦ起因過程のエネルギー放出挙動に関し実施した、ＣＡＢＲＩ－１を中心とする炉内試験の総合評価及びそれに基く解析評価手法の改善と、その実機評価における効果についてまとめたものである。

ＣＡＢＲＩ－１試験の評価では、実機の反応度挙動に特に重要となる、燃料の軸方向膨張、燃料破損及び破損後燃料運動現象に注目し、ＰＡＰＡＳ－２Ｓ、ＳＡＳ３Ｄ、ＳＡＳ４Ａコードを用い、広範なデータに対し詳細な解析を行なった。これにより現象を解明し、ＵＬＯＦ事象下でのエネルギー発生の抑制に働く自己制御機構の特性と有効性を明らかとした。

また、得られた最新の知見を改良版ＳＡＳ３Ｄコードの物理モデル改良に反映する事により、実機評価手法の改善を行なった。

以上の炉内試験データに基く知見と改善評価手法を中型炉心ＦＢＲのＵＬＯＦ事象解析に適用し、従来の評価手法による結果と比較することにより、本研究で得られた自己制御機構を安全解析に反映する事がエネルギー放出及び事象進展を現実的に評価する上で、重要かつ有効である事を確認した。

* 大洗工学センター、安全工学部、高速炉安全工学室

CONTENTS

LIST OF TABLES

LIST OF FIGURES

LIST OF FIGURES (continued)

1. INTRODUCTION

In the framework of the severe accident research efforts, the energetics potential in postulated core disruptive accidents (CDAs) has been one of major concerns in the safety of liquid-metal fast breeder reactors (LMFBRs). On this subject much efforts have been devoted to assessments of an unprotected loss-of-flow (ULOF) accident sequence with emphasis on the initiating-phase energetics, because the coherent accident progression potentially leads to a high power transient associated with a LOF-driven-transient-overpower (LOF-d-TOP) event.

In the area of safety experimental research on this issue, the international in-pile test program, CABRI-1 has provided extended database and valuable information for the phenomenological understanding and validations of safety analysis codes.[1, 2] On the key transient phenomena of axial fuel expansion, fuel failure and fuel motion, in particular, inherent mitigation mechanisms to energetic ULOF sequences are reinforced effectively under the fast transient domain, giving the self-limiting mechanisms to the accidents. These mechanisms were often neglected in the previous safety assessments because of the insufficient experimental evidences.

The present paper summarizes the improved understanding obtained through the CABRI-1 analyses with PAPAS-2S[2], SAS3D[3] and SAS4A[4] codes on the above three key phenomena. It also discusses the improvement of the evaluation method, which is introduced in the revised version of SAS3D, based on the CABRI-1 research efforts at PNC. Finally, the reactor application study is presented to examine the effect of the improved evaluation method on the ULOF accident progressions.

2. AXIAL FUEL EXPANSION

The axial fuel expansion behavior plays a key role in dominating the coherency of accident progression, in terms of the timing and rate of the core voiding, and the resultant power and reactivity conditions prior to the core disruption. Although this behavior potentially provides an inherently safe mechanism promptly responding to fuel heat-up like the Doppler reactivity, this effect has been neglected as a conservative assumption in reactor safety assessments due to lack of sufficient database with quantitative evidences. In this respect, the CABRI-1 experiments has introduced valuable data for improving the evaluation method.

In CABRI, the transient fuel expansion behavior was measured by the neutron hodoscope under various TOP and LOF-TOP conditions for fuel pins with different irradiation states.[1] Figure 1 presents the measured fuel expansion data at various transient states, e. g. boiling onset, TOP onset and failure time, comparing with evaluations with the PAPAS-2S code. The analyses giving overall agreement with the test data are based on the clad-constraint expansion mechanism where free thermal expansion is allowed until an extended hard contact with cladding. The subsequent expansion in the constrained mode is controlled by the cladding expansion which is much smaller than the free fuel expansion under TOP conditions. The validity of this mechanism can be seen in the figure as a general dependency on the test conditions. Namely, the maximum expansion is realized in the fresh-fuel TOP tests in which the wide initial gap between fuel and cladding leads to a delayed contact and high energy failure achieving the large expansion. The next group with moderate expansions up to 10 mm consists of the LOF-type tests where the free fuel expansion is assured during LOF, regardless of the irradiation conditions. The lowest potential is found for the pure TOP tests with the irradiated fuels because of the narrow initial gap for the test fuels. In the case of the extended LOF condition with a channel voiding progression, the

mechanically strengthless cladding at elevated temperature cannot constrain the fuel expansion even after the TOP onset, and the free thermal expansion continues until fuel stack disruption. Such a large expansion response representing a lead channel in LOF-d-TOP events, for instance, is indicated for the BGS0 test in Fig. 1.

The above mechanism for the axial fuel expansion supported by the extensive analyses with PAPAS-2S was fed back to the revised SAS3D expansion model for reactor analyses. In the new model, the fuel stack above the uppermost contact position freely expands axially, whereas the part below this position is assumed completely stuck without contribution of the cladding expansion. The modeled expansion behavior is schematically represented in Fig. 2 for a LOF-TOP case. This model was found to be appropriate in analyzing LOF-TOP conditions as seen in Fig. 3. Though the simple treatment of the stick condition may somewhat underestimate the CABRI test results, this seems reasonable for reactor applications because possible pin constraint due to the bundle geometry might reduce the cladding expansion.

The revised SAS3D model was applied to a reactor analysis for a ULOF accident. The result of reactivity behavior depicted in Fig. 4 indicates that the negative reactivity feedback due to the axial expansion works effectively and gives a comparable effect with the Doppler contribution, at least, until the power burst phase when the cladding constraint initiated in unvoided low-powered subassemblies (S/As) limits the fuel expansion.

Consequently, the important role of the axial fuel expansion as a self-limiting mechanism in ULOF accidents is verified with the qualified bases, and the former assumption of neglecting this reactivity effect is judged to be no longer reasonable for safety assessments.

3. FUEL FAILURE CONDITION

The fuel failure mode and condition influence decisively the post-failure materials relocation and thus consequences on the initiating-phase energetics. Main concerns on this phenomenon are: failure mode and its mechanism relevant to fuel mobility; fuel energy condition to determine failure timing; and axial failure position relative to the fuel reactivity worth profile. In the CABRI-1 program, energetic power pulses with fuel heating rate of 1 to 100 kJ/g/s were triggered under various cooling conditions, which systematically cover the variations of power-to-flow mismatch during LOF.

The fuel failure data accumulated in CABRI-1 have been also analyzed by PAPAS-2S. The results are summarized in Fig. 5 as a failure map showing the relationship between fuel failure energy and cooling condition, which clarifies the fuel failure modes dependent on the cladding thermal condition.

For the cladding temperature below about 1200 °C, the fuel pin fails in the burst mode (mechanical cladding rupture and fuel ejection into the coolant channel) with a high internal cavity pressurization because the strength of cladding is maintained up to that temperature level under rapid heating condition. The internal pressure loading required in this failure mode decreases with increasing the cladding temperature, in accordance with the characteristics of the temperature-dependent cladding strength obtained from the mechanical property test.[5] While the failure energy in the low cladding temperature range apparently depends on the pre-irradiation and heating-rate conditions, the actual loading parameters are sufficiently correlated with a linear relationship, shown in Fig. 6, as a general failure criterion representing the failure mechanism. The heating-rate effect on the failure energy can be clarified in Fig. 6, where the failure data combined with TREAT are compared in a wide heating-rate range. That is, as a general tendency, increased heating rate makes the failure energy high, though

the energy has a rather wide band affected by the fuel design and irradiation conditions . This heating-rate dependency is understood by the combined effects of the cladding strength and PCMI loading characteristics. For instance, within CABRI, the AGS3 test with a gas-rich and high smear-density fuel experienced both high cavity pressure and PCMI loadings under a low heating-rate condition and thus resulted in the lowest failure energy.

The initial failure in the burst mode is located above the axial midplane where the cladding is thermally weakened with a peaked strain damage typically under LOF-TOP conditions.[2] This is confirmed by the fact that the average relative height of failure in the five LOF-TOP tests is 0.68 with a standard deviation of 0.06. Because of a high potential of the failure extension,[2] it is stressed that the former assumption of localized midplane failure often adopted for conservative evaluations of the LOF-d-TOP event is physically unrealistic.

In the higher temperature range corresponding to post-dryout phase in Fig. 5, the cladding has no sufficient strength to constrain the fuel stack geometry, and the fuel disrupts in a relatively wide axial region. PAPAS-2S analyses for this failure mode suggested that the high fuel heating rate above ca. 5 kJ/g/s should cause a rapid fuel dispersion achieving a high mobility, which is mainly driven by the effective overpressurization of grain-boundary fission gas bubbles. Those findings and interpretations for CABRI data are fairly consistent with the observations in the visual in-pile tests, FD and STAR at SNL.[6] The observed characteristics of the fuel mobility upon the disruption are summarized in Fig. 8 together with test conditions in other experiments. The effects of the fuel energy condition based on the CABRI and SNL tests are expressed as sub-modes of disruption on the map. The improved knowledge on the enhanced mobility by increasing energy and its rate supports importance of the disruption phenomenon as a self-limiting mechanism to initiate a prompt fuel dispersal in voided lead S/As under an energetic ULOF sequence.

Another concern in this failure mode is the condition of disruption timing and axial extent to determine the amount of mobile fuel during transient. The PAPAS-2S analyses showed that observed response for irradiated fuels on initial disruption and subsequent progression contributing to the axial fuel relocation is well represented by the melting onset in gas-rich radial fuel section (unrestructured fuel zone for high-powered fuel structure), which is consistent with the above mechanism based on heat-up of the fission gases and mobility increase. As a result, the irradiated fuel attains mobile condition much earlier than the fresh one in terms of accumulated fuel energy level.

The failure mechanisms and conditions investigated with the test analyses were also incorporated in the revised SAS3D code by applying the revised failure criteria, and its capability for evaluating the failure conditions was validated also in CABRI LOF-TOP test analyses. Figure 9 compares the fuel disruption pattern in the BI3 test between the hodoscope measurement and the analysis by the revised model. Figure 10 gives the time histories of the loading parameters and failure predictions in the analyses of the sodium-constrained failure test BI2, where the revised method well predicted both the timing and position of the failure. Also indicated in the figure is the importance of consistent treatment of the axial fuel expansion, which sensitively affects the internal pressure loading through the cavity volume change.

The improved understanding and evaluation method on the fuel failure phenomenon provide reliable bases for initial conditions to evaluate the post-failure materials motion behavior. At the same time, these can effectively update the former method in reactor assessments, like simplified failure criteria based on the fuel melt fraction.

4. POST-FAILURE FUEL MOTION

The fuel motion phenomenon has a definitive role in determining the final entry condition to the LOF-d-TOP event and consequences of the ULOF initiating phase, since it has a significant reactivity effect which most potentially compensates the positive reactivity insertion due to core voiding. In addition the core-material configuration as a initial condition for the transition phase after energetically benign sequences owes much to the phenomena. For reliable evaluations of the relocation behavior, it is essential to understand, based on wide experimental evidences, the effects and roles of driving forces and interactions of the mobile fuel with coolant and structures as well as its quality and amount.

For the different failure modes mentioned above, the CABRI tests have been selectively analyzed with PAPAS-2S, SAS4A and SAS3D with a special focus on the early fuel motion mechanism.

4.1. Fuel Motion in Voided Channel

With regard to the fuel motion in an extended-void channel, the previous study on fresh fuel tests revealed the effectiveness of steel vapor pressurization for driving the early fuel dispersive motion under energetic power bursts.[2] A typical example is shown in Fig. 11, where the transient fuel worth change in the B5 fresh fuel test is compared with the SAS3D and SAS4A analyses. In addition to this driving force, the burnup effect was examined by analyzing irradiated fuel tests. Figure 12 shows the transient fuel relocation characteristics in B13 test analyses by the revised SAS3D code, where the normalized worth changes based on the hodoscope data and two calculated results are compared. Difference between the two cases is for the fission gas contribution, while the steel vapor and sodium streaming effects are taken into account in the same manner. The reference case,

simulating the fast fission gas release from melting fuel with a time constant of 10 ms, explains the test result much better than the other case which assumes no availability of the grain-boundary gases upon disruption and the delayed release by a 100-ms time constant. Judging from the result that the calculated axial progression of the disrupted area showed a good agreement with the measurement thus giving a proper condition for the mobile fuel mass, the analyses confirm the significant contribution of the fission gases to drive the early fuel dispersal. The accelerated gas release by fuel melting is also supported by several separate-effect experiments like SILENE.[7] As seen in Fig. 12, a general trend from the CABRI tests is that the dynamic relocation of the irradiated fuel is initiated within 20 ms after the disruption onset when the fuel energy reaches 1.1 to 1.2 kJ/g, which is clearly below the energy level for fresh fuel and far below the fuel vaporization energy.

Another aspect of the extended fuel relocation is the interaction between moving fuel and liquid sodium near the lower void boundary, which has been well reproduced in the CABRI LOF-TOP tests. According to examinations with SAS4A analyses, this type of interaction generates a steep pressure gradient through the rapid sodium vaporization process and further accelerates the upward fuel dispersal and penetration into the colder structure.[2] This dispersal potential by the sodium vaporization is not sufficiently treated in SAS3D, which tends to underestimate the upward relocation because only a weak coupling with the streaming sodium vapor can be simulated regardless of the fuel-sodium mixing condition. The somewhat delayed dispersal in the BI3 reference case is believed to be ascribed mainly to the underestimated sodium-vaporization effect, and its contribution to the extended fuel motion becomes more significant in higher energy injection cases because of efficient mixing and sodium vaporization. It is noticed, therefore, that further modeling and quantification efforts are necessary

to realistically introduce such an effective mechanism typically under energetic LOF-TOP conditions.

The integral CABRI data on the disruption failure mode clearly indicated that the fuel dispersal and fuel removal out of the original fissile area are enhanced with the increased energy and heating rate, and that effectiveness of the energy dependency is superior to that in the constrained failure mode under less advanced LOF conditions. These aspects are shown in Fig. 13. The former characteristic response, which reveals the vital importance as a self-limiting mechanism to the energy release, is understood by considering combined effects discussed above. Namely, energetic LOF-TOP sequences promote extensive and dynamic fuel disruption achieving highly mobile condition on one side, and produce diverse and enhanced driving forces by fission gases, steel and sodium vapors, on the other side, leading to the early and extended fuel dispersal. The latter general aspect on the channel cooling condition implies a relative importance, during ULOF accidents, of the role of high-powered lead S/As, where a hot channel condition helps maintain the high fuel mobility and alleviate impeded flow-path formations through fuel freezing by interactions with cold structures. Hence the fuel fluidized early in the lead S/As has a high potential to respond quickly to a later power transient. Consequently, the self-limiting mechanism validated in the CABRI experiments and analyses should be taken appropriately into account to reflect the causal relations between transient conditions and governing phenomena on evaluations of ULOF accident progressions. In this connection, the previous assumption to neglect the early relocation mechanism until the fuel vaporization has no physical basis, and its application to reactor analyses may largely distort the actual accident progression under a ULOF.

4.2. Fuel Motion in Non- or Partially-Voided Channel

In the burst failure mode with the cladding constraint, the fuel motion starts with intra-pin motion towards a failure rip with rapid fuel ejection into the coolant channel and , which are driven by the molten-fuel cavity pressure. In CABRI, this initial fuel motion upon the failure are clearly observed by the hodoscope and coincidently followed by a sharp pressure event and the resultant sodium flow transients which drive the axial fuel motion in the coolant channel. Hence the driving pressure due to the fuel-coolant interactions is one of keys to evaluate correctly the fuel relocation behavior.

The comparative analyses by PAPAS-2S and SAS3D on failure tests in an unvoided channel have pointed out that the one-point interaction-zone model adopted in SAS3D overestimates fuel-sodium heat transfer and thus interaction zone pressure. This results in too fast void expansion during a decompression phase.[2] This problem was corrected in the revised SAS3D by introducing an enhanced vapor-blanketing model for which model parameters were calibrated against measured pressure-volume works. The revised model much improves the pressure and flow transients, and give a reliable basis for evaluating the void reactivity and fuel relocation behavior under energetic power burst conditions.

Also indicated in the analyses is that during the early dynamic phase up to about 20 ms accompanied by the rapid two-phase zone expansion, axial velocity profiles of fuel and gaseous components develop linearly without large slip. This result obtained by the two-fluid model in PAPAS-2S supports the applicability of the simplified SAS3D model for analyzing the early fuel relocation phase.

Another important mechanism to influence the fuel motion is the transient extension of the failure rip. Particularly under energetic LOF-TOP conditions, possibility of early failure extension is increased because the cladding damage tends to develop along a wider axial region,[2] under the sustained internal-

pressure loading, by rapid heat-up process due to the void formation and additional heat transfer from the coolant-channel fuel. To cope with this mechanism, SAS3D was modified such that the pressure burst criterion described in the previous chapter is continuously applied also accounting for the channel pressure response to simulate the rip extension within the interaction zone.

As discussed earlier, the channel cooling condition affects sensitively the fuel relocation behavior. As is often the case with ULOF conditions, fuel pins in intermediate-powered S/As fail into partially voided channels where coolant boiling is already started and the void region is extending towards the axial position to be failed. It is found in CABRI that this situation brought noticeable effects on the hydrodynamic response and the fuel relocation behavior after the failure, compared with those under the unvoided condition.

To investigate these effects in detail, the BI4 LOF-TOP test was analyzed in parallel with the revised versions of SAS3D and SAS4A. The initial failure site in BI4 is located at the relative fissile height of 68 % which is just below the lower void boundary. The calculated results of the fuel worth changes and the axial fuel relocation patterns at two time windows are compared with the hodoscope data in Figs. 14 and 15, respectively. As shown in the figures, the upward fuel relocation starts immediately after the failure and this leads to a prompt and high-rate reduction of the fuel worth. Both the codes well explain the hodoscope data on the early dynamic fuel relocation phase during the first 30 ms. Intensive examinations of the analyses clarified that this effective fuel dispersal had originated from the several combined mechanisms: rapid intra-pin fuel motion towards the high ejection site; upward acceleration of the ejected fuel by the steep pressure gradient formed within the interaction zone because of the short liquid slug below the upper boiling region; and early upward failure-rip extension due to the severe heating of the upper hot cladding region by prompt upward voided-zone expansion and massive moving fuel in the coolant channel. In

particular, the effect of the small inertia of the short liquid slug is so large that the most channel fuel relocates upwards in the early phase. The failure extends up to 10 cm above the initial site within 10 ms and this augments the momentum coupling of the continuously ejected fuel in the steep pressure gradient. These interpretations supported by the experimental evidences and analysis with SAS4A verify the high potential of fuel dispersal under the partially voided condition, and capability of the revised SAS3D code for evaluating the early dynamic relocation phase in this failure mode.

In the later long-term relocation phase, however, SAS3D tends to underestimate the continued fuel dispersal especially in the sodium-flow deceleration phase, showing the clear difference from the SAS4A result as shown in Fig. 14. This is also ascribed to the fact that cladding ablation and fuel stack disruption are not taken into account, which may enlarge the fuel flow area and increase the mobile fuel mass in the channel. The SAS4A analysis treating these effects as well as the transition of fuel flow regimes and plate-out freezing on cold structures systematically explains the hodoscope data, indicating: fuel removal from the hot fissile region with a high fuel worth, accumulation just below the fissile top and penetration into the upper blanket region [see Fig. 15-(2)]. Also indicated in the analysis is the significant effect of the cold outer structure, which is one of the conditions specific to the CABRI single-pin geometry. Namely, the upper fuel accumulation shown in Fig. 15-(2) results from the rapid convective heat transfer to the structure from the molten fuel which enters into the still intact fuel region and then is frozen quickly there. Although the current SAS4A model overestimates the fuel freezing rate, the general behavior in the analysis appears consistent with observations in the post-test examinations. Even with the structure effect, the extensive fuel dispersal was achieved within 100 ms after the failure, and this again proves the importance of the LOF-induced cooling conditions of fuel pins as indicated in Fig. 13.

Consequently, it is clarified in this study that the inherent mechanisms strengthened by the partially voided condition have a significant contribution to limiting the energetics potential under ULOF, and that the improved SAS3D is applicable to the early phase of the post-failure phenomena, which is one of main concerns for assessing the LOF-d-TOP event. Nevertheless, it is noticed at the same time that the long-term fuel motion including the penetration behavior out of core region needs more systematic and mechanistic modeling of the interactions between the core materials, like in SAS4A, to be realistically evaluated for energetically benign ULOF sequences.

5. APPLICATION TO REACTOR ANALYSES

The improved evaluation method implemented to the revised SAS3D code, based on the phenomenological understanding accumulated and validated through the investigations and analyses of the CABRI-1 and relevant safety experiments, was applied to reactor analyses for a ULOF initiating phase.

5.1. Improved Evaluation Method and Analytical Conditions.

In this study, typical energetic sequences were simulated by postulating conservative void and Doppler reactivities to a medium-sized two-zone homogeneous core at the end-of-equilibrium-cycle state. To clarify the effects of the improved method on the reactor accident progression, an analysis by the previous method, which has been usually employed in safety assessments since late 1970's, was also carried out. Namely, two cases based on the up-to-date best-estimate approach and the conventional one are compared in the analyses.

The major improved knowledge and relevant physical modeling applied to the new evaluation method are summarized in TABLE I comparing with the previous method. As indicated in the table, the previous method superimposes pessimistic assumptions on the key phenomena, i.e. axial fuel expansion, fuel pin failure and early fuel motion, while the improved method reflects widely the knowledge obtained in the last decade. For the latter analysis, the plenum-gas driven fuel-stub motion is remodeled taking an upper-plenum design into account, though in the CABRI-1 tests using a lower-plenum fuel pin such a motion is found to occur only late in the transient after the dynamic fuel relocation phase.[8]

The main design characteristics of the reactor analyzed and related conditions of ULOF are shown in TABLE II.

5.2. Results and Discussions

The results of the two analyses employing a 14-channel lumping scheme are compared in Fig. 16 on net reactivity and reactor power histories. It should be noted that the common reference time to the both cases is taken at fuel motion onset and the time scale is enlarged for the high-power transient domain. In the following the case with the improved method is referred to as Case A, and the other as Case B.

At 15.8 s after the LOF initiation with a flow halving time constant of ca. 5 s, the coolant boiling starts in Case A. This is about 2 s later than Case B because of the effective axial fuel expansion. The high void reactivity condition assumed drives a sharp reactivity increase with core voiding progression (coolant reactivity: 0.6-0.7 $/s), and the resultant power escalation initiates fuel disruptions in the voided high-powered channels under high-heating rate conditions above 10 kJ/g/s. The subsequent progressions reveal much pronounced differences between the two cases because of the self-limiting mechanisms.

In Case B, the potential of the early fuel dispersal in the lead channels is neglected. This case leads straightforward to the prompt criticality with a low core void fraction (about 25 %), because there is no effective mechanism to compensate the void reactivity insertion except for the reduced Doppler effect. On the moment, a highly coherent LOF-d-TOP event is triggered by the midplane failures in a wide core area (70 % S/As) including medium-powered channels. This further boosts the reactivity ramp rate up to about 60 $/s, which is mainly caused by the intra-pin fuel motion towards the fixed midplane failure site, and results in an energetic power burst. Then the delayed fuel dispersal by the fuel vaporization in the lead channels becomes effective and decreases the net reactivity, finally shutting down quickly the reactor as a result of the severe core heating.

On the other side in Case A with the revised method, the high fuel heating rate upon disruption in the lead channels enhances the fuel mobility and pressurization by the rapid fission gas release and vaporization of the cladding steel, and then initiates the early fuel dispersal. This effective negative-reactivity response to the power increase, combined with the still increasing axial expansion effect, keeps the reactor sub-prompt-critical, compensating sufficiently the high-rate void reactivity insertion. Subsequently at 20 ms after the fuel disruption onset, the net reactivity begins to decrease because of the extending area for disruption and dispersal in the high-powered channels. Hence the early fuel dispersal prevents the LOF-d-TOP event in this initial core disruption phase and guides the accident to non-energetic sequence. However, shortly after the pins in a medium-powered channel start to co-disrupt with cladding, the unrelieved plenum-gas pressure accelerates the upper intact fuel stub downwards until the channel pressure increases in the disrupted region. This compactive fuel motion is activated rather coherently in this case because of the rough channel lumping scheme, e.g. 15 S/As in this channel concerned. This contributes to re-increasing the net reactivity towards the prompt-critical condition causing a secondary power escalation. Nevertheless, since by this time core voiding already prevails in an extended region (50% core-average void fraction) where a large amount of mobile fuel is available, this power increase is subtly followed again by the effective fuel dispersal in the voided channels, which limits the reactivity ramp rate at the prompt criticality. The extended core voiding also mitigates the potential of an energetic LOF-d-TOP event because of the narrowed triggering region and much reduced void reactivity to be added through the fuel-coolant interactions. That is, most of the positive void reactivity, about twice as much as in Case B, has already been compensated by the other negative components. Therefore, even though the LOF-d-TOP event takes place in a core periphery, the fuel pins fail incoherently above the midplane and mostly under the partially voided condition. In this failure

condition, additional reactivity insertion is insufficient to maintain the prompt criticality, and the effective fuel dispersal promoted by rapid failure extensions rather decreases the net reactivity shortening the prompt-criticality duration. Accordingly, the reactor is guided to a deep subcriticality with an assistance from the large-scale fuel dispersal in a central voided-core region, which results in a much milder core energy release than in Case B without threatening the integrity of reactor boundary system.

The main results on the energetics potential in the two cases are summarized in TABLE III. As confirmed in the table, the self-limiting mechanisms provided for the improved method has a vital importance in mitigating the energetics potential under the ULOF condition: i.e. the maximum reactivity ramp rate upon reaching the prompt critical and the resultant core expansion energy up to the slug impact are reduced by about factor of three in CASE A.

It is worth mentioning that the coherent fuel compaction due to the plenum-gas pressure in Case A is much alleviated in an additional 33-channel lumping case[CASE A'], which more precisely reflects the in-core distributions of the power-to-flow ratio and fuel burnup condition. The result of CASE A' is compared with that of CASE A in Fig. 17, which shows that in the detailed lumping case the accident progresses non-energetically without LOF-d-TOP event. Subsequently, this case enters into the transition phase with low power and shallow subcriticality conditions, while the configuration of core materials indicates a wide variation in the lateral direction of the core providing a significant incoherency for possible recriticality processes during the early transition phase. This result implies the importance of sufficient representation of core-wide incoherency linked closely with the key phenomena in assessing realistically the broad accident sequences.

Therefore, it is verified in the application analyses that the improved method representing the self-limiting mechanisms by appropriate physical models brings large impacts on the accident progression for a ULOF and consequences of the

initiating-phase energetics, and that the previous method has no rational basis since it ignores essential parts of the causal relations between the key phenomena sensitive to reactor transient conditions.

6. SUMMARY AND CONCLUSIONS

The extensive analyses of the in-pile experimental database accumulated in the CABRI-1 international program have been made on the three key phenomena to the initiating-phase energetics, i.e. axial fuel expansion, fuel failure and post-failure fuel motion. In this study, the important mechanisms, originating particularly from LOF conditions, to limit inherently the energetics potential are clarified to a great degree with the experimental evidences, which gives the improved understanding of phenomena essential to evaluate the high power transient. These are: the high potential of axial fuel expansion during LOF; the diverse and effective mechanisms to drive the early fuel dispersal in voided channels; the above-midplane failure and early extension including the transition to the fuel stack disruption; and the resultant dispersive fuel motion reinforced by the partially voided conditions.

Meanwhile, the improved knowledge based on the analyses of CABRI-1 and other safety experiments has been implemented to the revised version of the SAS3D whole-core analyses code at PNC as an improved evaluation method for the initiating-phase energetics in ULOF. The capability and characteristics of the revised SAS3D on the relevant phenomena have been extensively examined and validated also against the CABRI-1 experiments, with the supports by comparative analyses using the detailed physical models in PAPAS-2S and SAS4A.

The improved evaluation method introduced in the revised SAS3D was applied to the reactor analyses for a ULOF accident. The results clearly showed with an enhanced confidence level that the self-limiting mechanisms functions very effectively to make the accident progression slower. This narrows down the entry condition to an energetic LOF-d-TOP event and mitigates the energetics potential, if any, compared with the previous evaluation method. It is concluded, therefore, that the superimposed pessimistic assumptions on the key phenomena which have

been often adopted in previous safety assessments are not of rational basis any longer from the viewpoint of the present status of technology, and that an appropriate evaluation method to represent the causal relations between the key phenomena and reactor transient conditions is a prime requirement for reliable assessments of the accident progression in CDAs. These knowledge and experiences obtained in the present research efforts are fed back extensively to the PSA study at PNC.[9]

Also identified in this study are the next-step research areas. One of the most important aspects is how the current knowledge obtained in the CABRI-1 fast transient domain can be extended or related to the milder transient domain, which represents energetically-benign accident sequences. In particular, the fuel failure response and subsequent long-term materials motion behavior of high burnup fuels under prolonged energy injections are the key concerns from the phenomenological viewpoint. A main part of the research program in CABRI-2 is oriented to this issue.[10] The data integrated with CABRI-1 are expected to further improve the current knowledge for development and qualification of the next-generation evaluation method founded with advanced mechanistic models like in SAS4A.

ACKNOWLEDGMENTS

The authors would like to express their profound gratitude to the members of the CABRI experimental team and the experimental program working-group for their excellent work on the in-pile experiments and the collaborative contributions to data evaluations.

The authors are also indebted to the staff of the FBR Safety Engineering Section, PNC for their direct or indirect contributions to this study.

The SAS3D and SAS4A codes were introduced from the Argonne National Laboratory under the agreement with the U.S. Department of Energy.

REFERENCES

1. G. HEUSENER, et al., "The CABRI-Programmes: Motivations and Achievements," *Int. Fast Reactor Safety Mtg.*, Snowbird, Utah, August, 1990.

2. N. NONAKA, et al., "In-Pile Experiment Analyses Relevant to Initiating-Phase Energetics," *Int. Conf. on Science and Technology of Fast Reactor Safety*, Guernsey, Channel Islands, May, 1986.

3. J. E. CAHALAN and D. R. FERGUSON, "A Preliminary User's Guide to Version 1.0 of the SAS3D LMFBR Accident Analysis Computer Code," Argonne National Laboratory, 1977.

4. A. M. TENTNER, et al., "The SAS4A LMFBR Whole Core Accident Analysis Code," *Int. Mtg. on Fast Reactor Safety*, Knoxville, Tennessee, April, 1985.

5. M. BALOURDET and R. CAUVIN, "Transient Mechanical Property of CABRI-1 Cladding," *Int. Conf. on Fast Reactor Core and Fuel Structural Behavior*, Inverness, UK, June, 1990.

6. S. A. WRIGHT, et al., "In-Pile Determination of Fuel Disruption Mechanisms under LMFBR Loss-of-Flow Accident Conditions," *Nucl. Tech., Vol.71, p.326* (1985).

7. J. L. FAUGERE, et al., "New Results on Fission Gas Release and Molten Fuel Pressurization Studies in the French Pulsed Reactor SILENE," *Int. Conf. on Science and Technology of Fast Reactor Safety*, Guernsey, Channel Islands, May, 1986.

8. D. STRUWE, et al., "Two-Phase Flow, Clad Melting and Transient Materials Relocation in the CABRI-1 Experiments," *Int. Fast Reactor Safety Mtg.*, Snowbird, Utah, August, 1990.

9. S. KONDO, et al., "Integrated Analysis of In-Vessel and Ex-Vessel Severe-Accident Sequences," *Int. Fast Reactor Safety Mtg.*, Snowbird, Utah, August, 1990.

10. M. HAESSLER, et al., "The CABRI-2 Programme - Overview on Results," *Int. Fast Reactor Safety Mtg.*, Snowbird, Utah, August, 1990.

TABLE I
Summary of Improved Knowledge and Comparison of Evaluation Methods for ULOF Analyses

Phenomena	Improved knowledge	Database [validation]	Analytical conditions and criteria applied for SAS3D	
			Previous method [original version]	*Improved method [PNC-revised version]*
Axial fuel expansion	free thermal expansion during LOF and limitation by clad constraint after power burst	CABRI-1	no expansion	*expansion controlled by clad constraint*
Fuel failure:				
in voided channel	disruption by pressurization of grain-boundary gas	FD*, STAR* CABRI-1	50% fuel areal melting	*melting onset of unrestructured fuel and loss of clad strength*
	increased fuel mobility under high power condition	(*: ACRR)	constant droplet size	*droplet size dependent on heating rate on disruption*
in unvoided channel	burst failure by intra-pin pressure with elevated clad temperature leading to above-midplane failure	CABRI-1, 2 TREAT-PFR	50% fuel areal melting (fixed midplane failure)	*correlation between intra-pin pressure and clad temperature (above-midplane failure)*
	rapid failure extension under high power transient	CABRI-1	no extension	*rip extension within voided zone*
Materials relocation in voided channel: clad motion	delayed motion onset due to surface tension and gas blowdown effects	STAR*, TREAT CABRI-1	early onset by melting	*delayed onset by high superheat and reduced coupling with two-phase flow*
fuel motion	effective early fuel dispersal by fission gases and steel vapor	CABRI-1 TREAT	fuel vapor as unique driving force neglecting early dispersal potential	*adopted early dispersal potential by pressure sources with increased fuel mobility*
	rapid gas release on fuel melting	SILENE, FGR FD*, CABRI-1	slow gas release by tc (time constant) of 100ms	*fast gas release by tc of 10ms and prompt availability of grain-boundary gas*
	delayed but significant driving force by interaction with liquid sodium	CABRI-1	no interaction assumed	*weak coupling with sodium vapor flow*
plenum-gas driven fuel stub motion	stub constraint by CsX accumulation motion onset after dynamic fuel relocation phase	irradiation data CABRI-1	no consideration(only gravity effect)	*considered with plenum pressure decrease and constraint effect for high burnup fuel*
MFCI and fuel relocation in unvoided or partially voided channel	enhanced blanket effect with expansion of interaction zone during high-rate fuel ejection	CABRI-1	limited blanket effect(over-estimated void extension)	*accelerated reduction of heat exchange dependent on sodium void fraction*
	efficient upward fuel dispersal due to failure extension and steep pressure gradient in case of partially voided channel	CABRI-1, 2	no consideration	*simulated by failure rip extension but no consideration for transition to disruption mode*
	fuel accumulation in axial edges of fissile under mild power burst	CABRI-1, 2	no consideration	*simulated by slip with sodium flow(onset by increased fuel volume fraction on cold structure)*

TABLE II

Main Characteristics of Reactor Design and Analytical Conditions

REACTOR DESIGN:

GENERAL:

Nominal Reactor Power	714 MWth
Fuel Average Burnup	80,000 MWd/MT
Core Height	93 cm
Core Equivalent Diameter	178.8 cm
Peak Linear Heat Rating	394 W/cm
Inner/Outer Core Pu Enrichment	16.1/20.8 % Pu-fission/(Pu+U)
Coolant Inlet/Outlet Temperature	397/529 °C

FUEL DESIGN:

Number of Fuel Assemblies	198
Number of Fuel Pins/Assembly	169
Fuel Pin Pitch	7.9 mm
Cladding Outer Diameter	6.5 mm
Cladding Thickness	0.47 mm
Fuel Pellet Diameter	5.4 mm
Fuel Pellet Density	85 %TD
Gas Plenum Position	upper
Fuel Pin Spacer	wire wrapping

NOMINAL CORE REACTIVITY COEFFICIENT AT EOEC STATE:

Maximum Void Worth	2.52 $
Core Fuel Doppler	
Sodium-in	-6.8×10^{-3} Tdk/dT
Sodium-out	-5.0×10^{-3} Tdk/dT
Axial Core Expansion	-0.64 $/cm
Beta Effective	3.64×10^{-3}
Prompt Neutron Life Time	0.438×10^{-6} S

ULOF ANALYTICAL CONDITIONS:

Pessimistic Reactivity Coefficients	+50 % of Void Worth and -30 % of Dopper Coefficients
Coolant Flow Coast-down	5 S of Flow Halving Time

TABLE III

Comparison of Calculated Results on Energetics Potential.

(SAS3D 14-Channel Analyses)

	Previous Method	Improved Method
Maximun Reactor Power (Po)	4400	880
Maximum Net Reactivity ($)	1.083	1.028
Maximum Reactivity Ramp Rate ($/S)	59	19
Average Core Fuel Temperature (K)	4860	3700
Core Expansion Energy* (MJ)	120	40

*: Isentoropic fuel vapor expansion work up to slug impact on shield plug

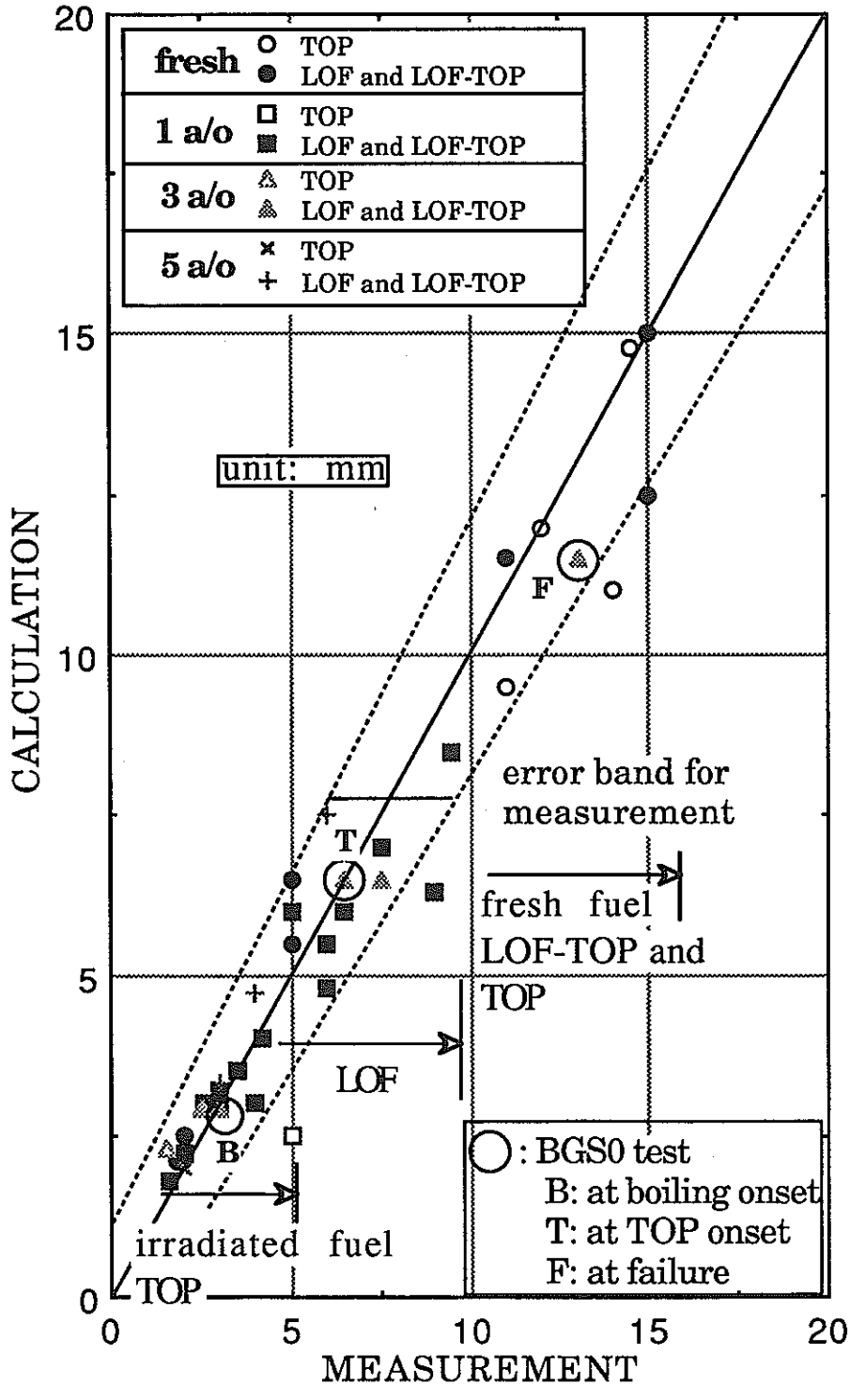

Fig. 1. Compparison between Measured and Calculated Fuel Expansion Results (test condition dependency).

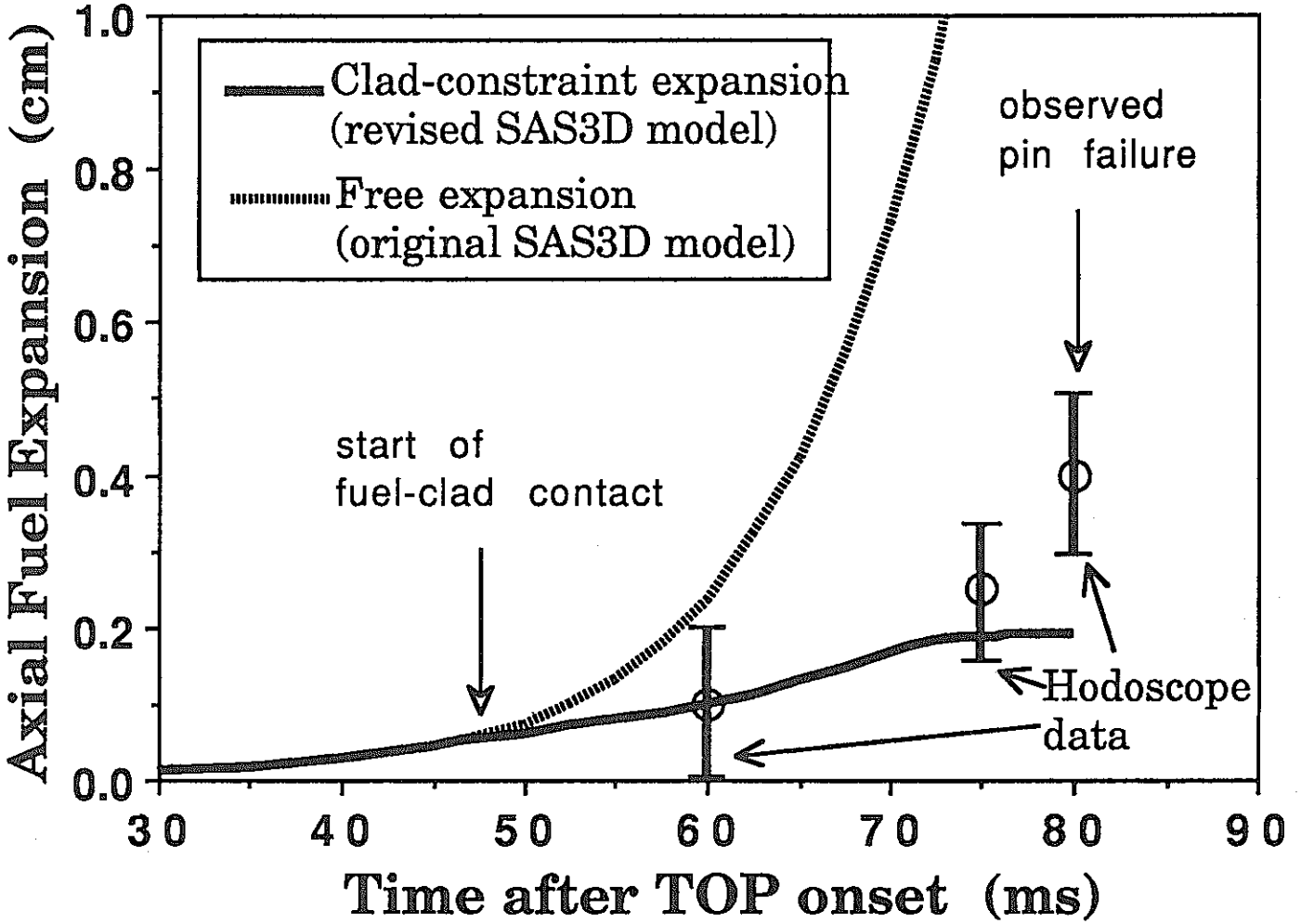

Fig. 2. Fuel Expansion Behavior during TOP Phase in BI2LOF-TOP Test.

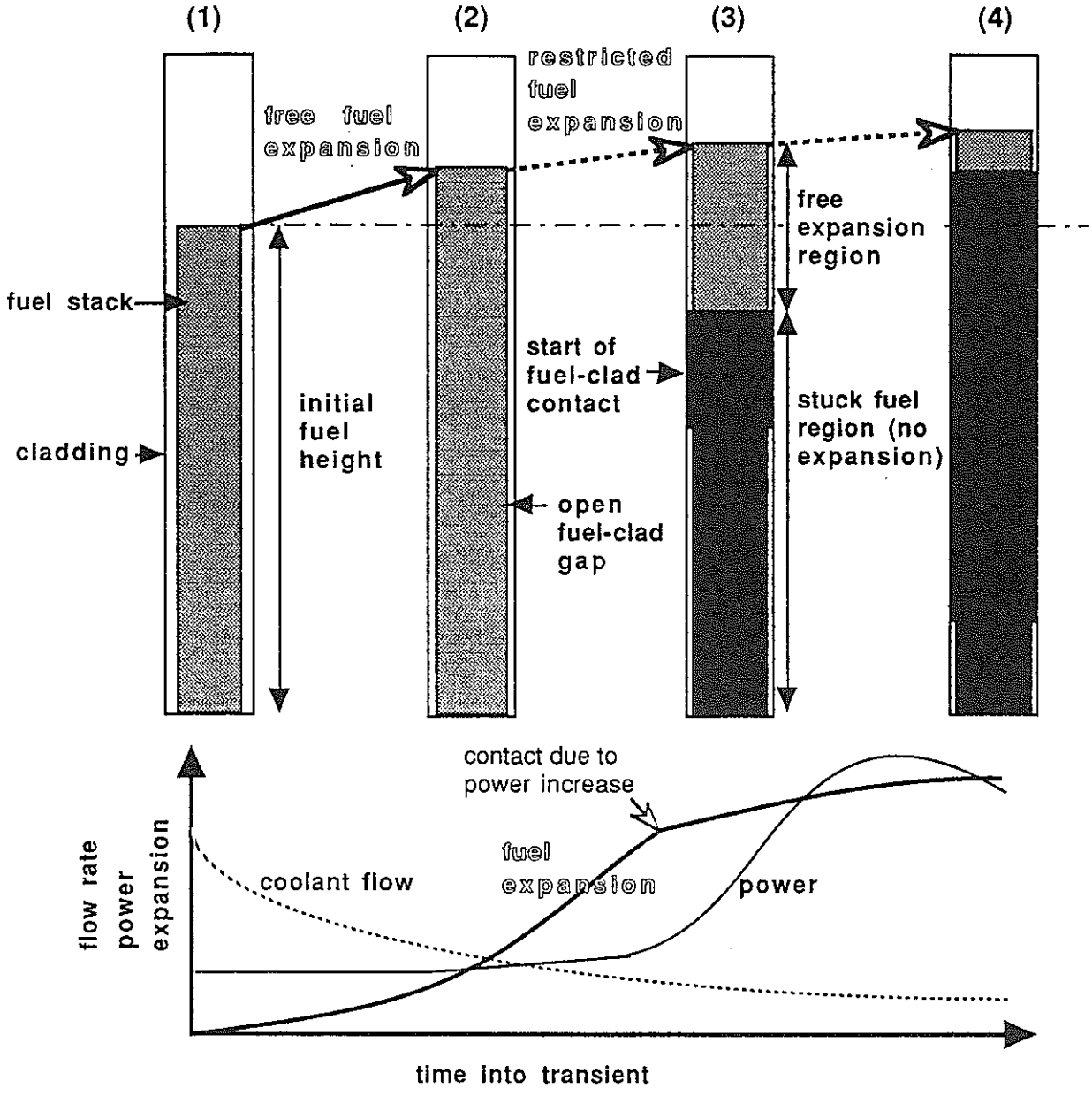

Fig. 3. Schematic Representation of Refined Fuel Expansion Model in SAS3D (introduction of cladding constraint effect).

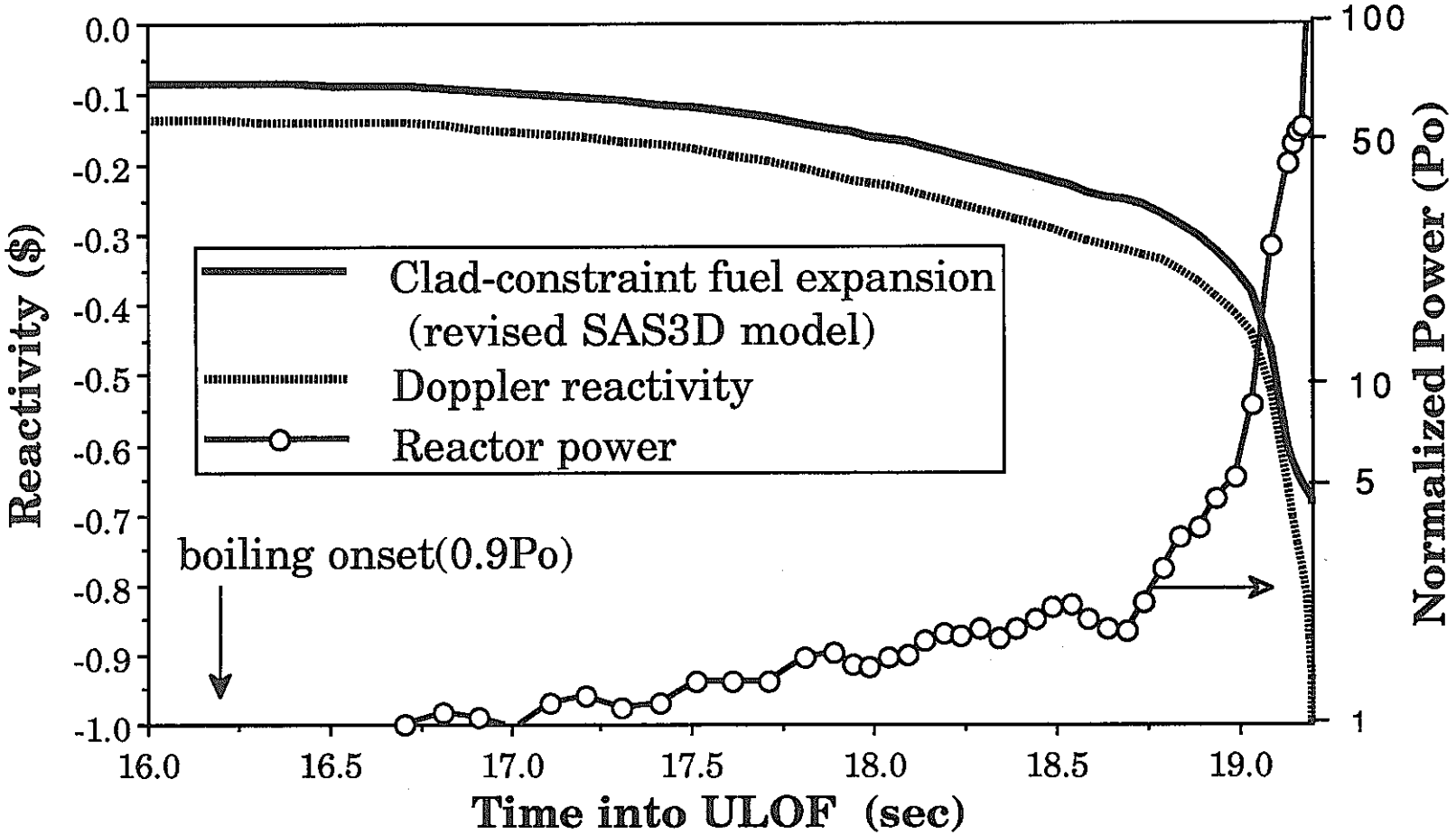

Fig. 4. Fuel Expansion and Doppler Reactivity Responses in Sample Reactor Analysis.

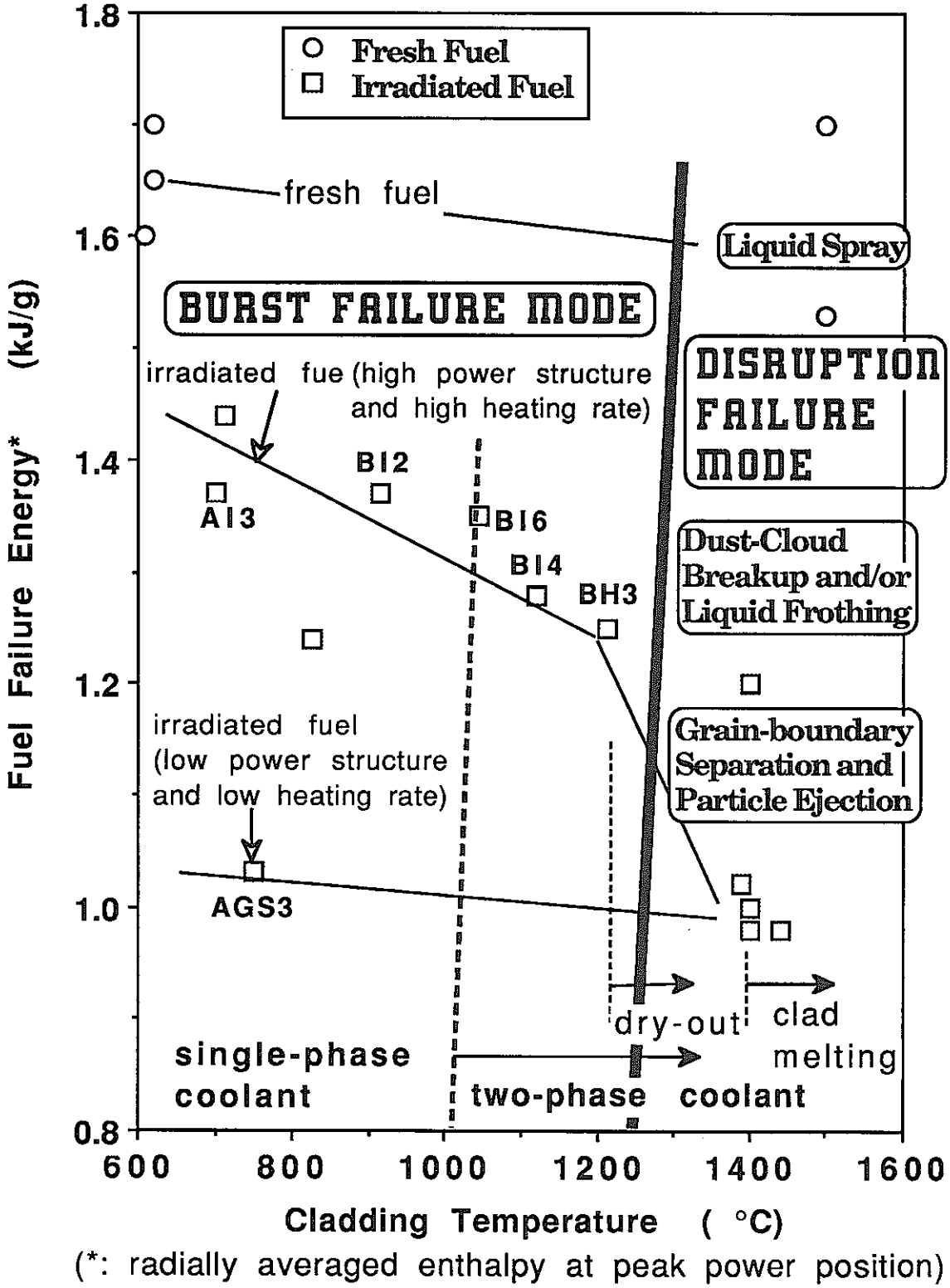

(*: radially averaged enthalpy at peak power position)

Fig. 5. CABRI-1 Fuel Failure Map.

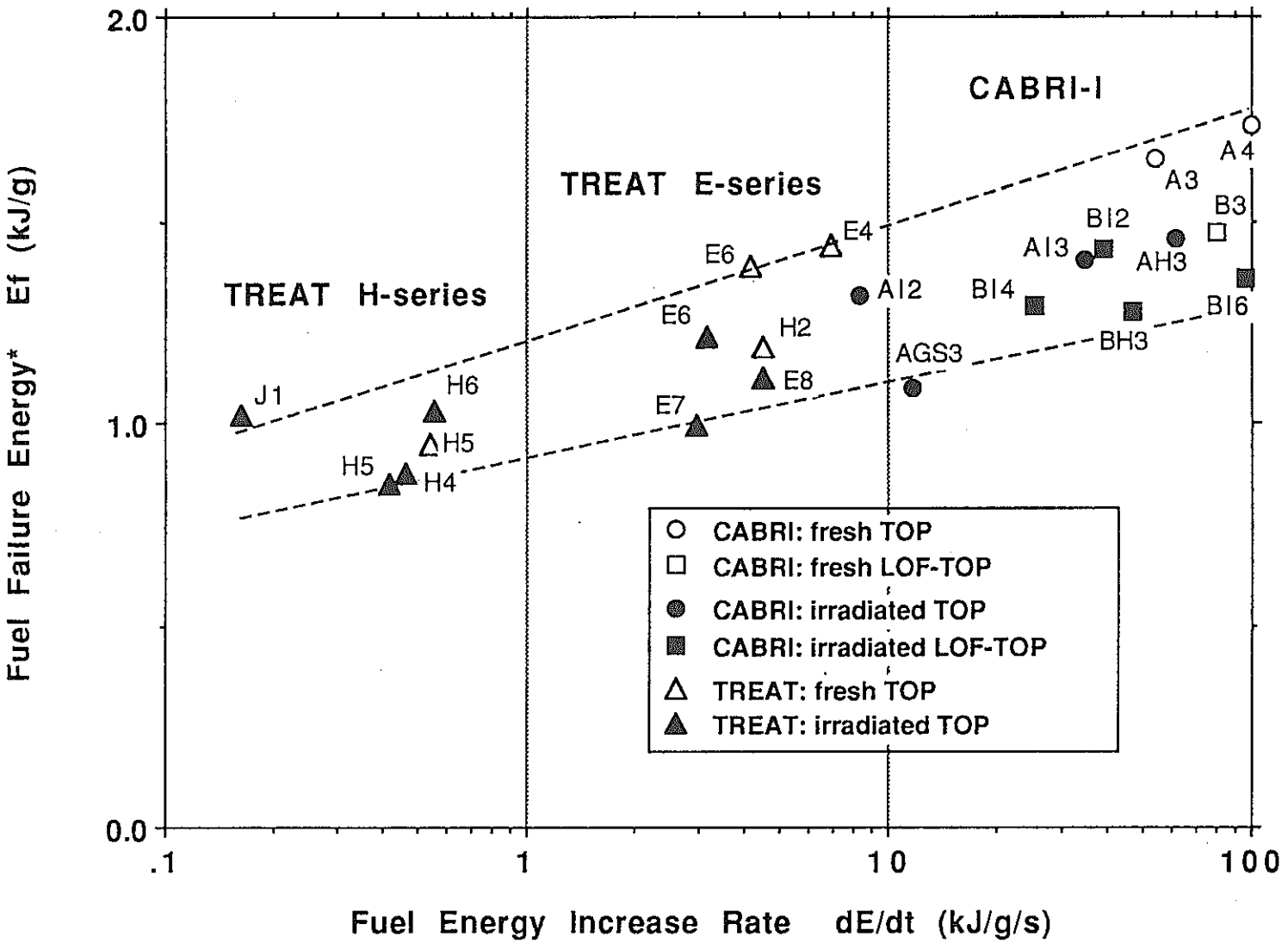

(*: radially averaged enthalpy at peak power position)

Fig. 6. RELATIONSHIP BETWEEN FUEL FAILURE ENERGY AND ENERGY INCREASE RATE UNDER RESTRAINED COOLANT CHANNEL CONDITIONS.

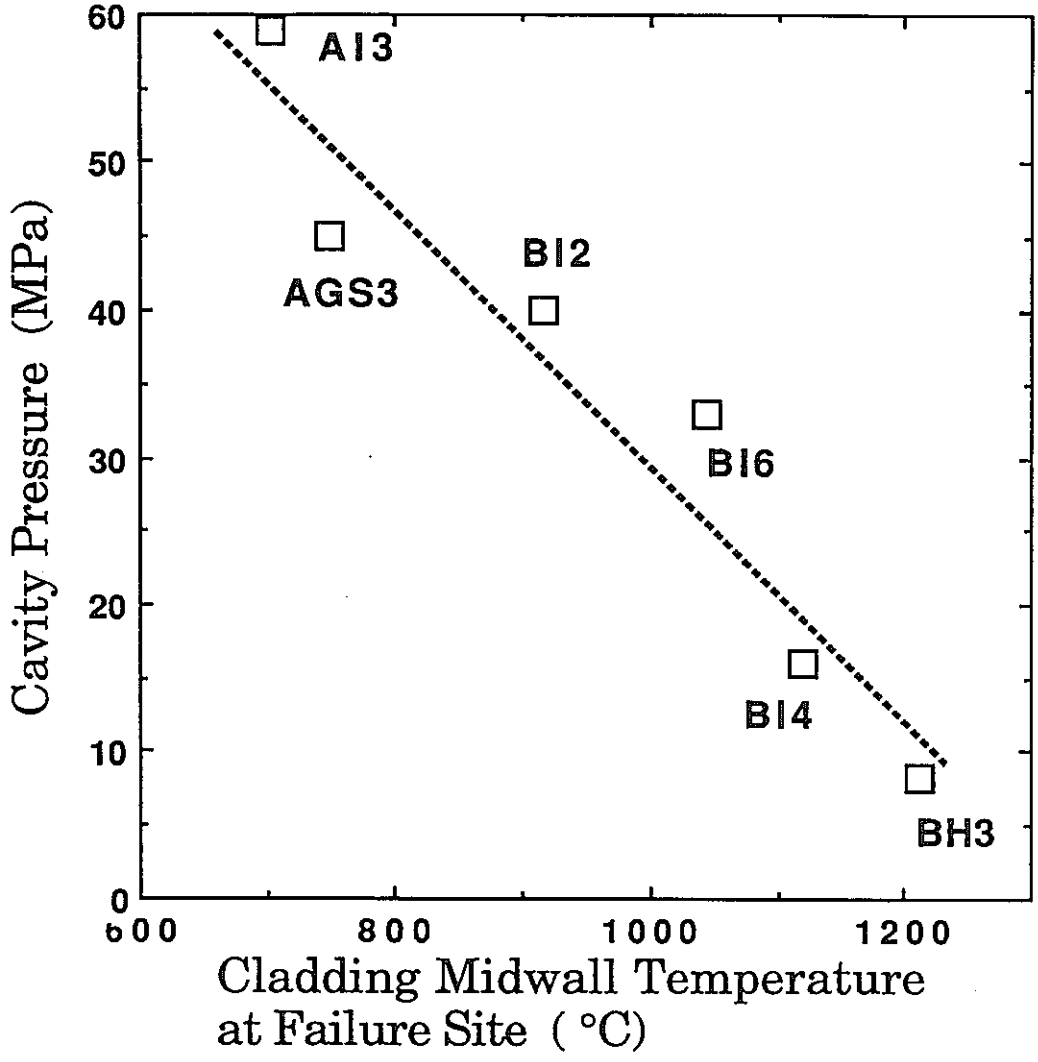

Fig. 7. Relationship between Cavity Pressure and Cladding Temperature Calculated by PAPAS-2S for Burst Failure Tests.

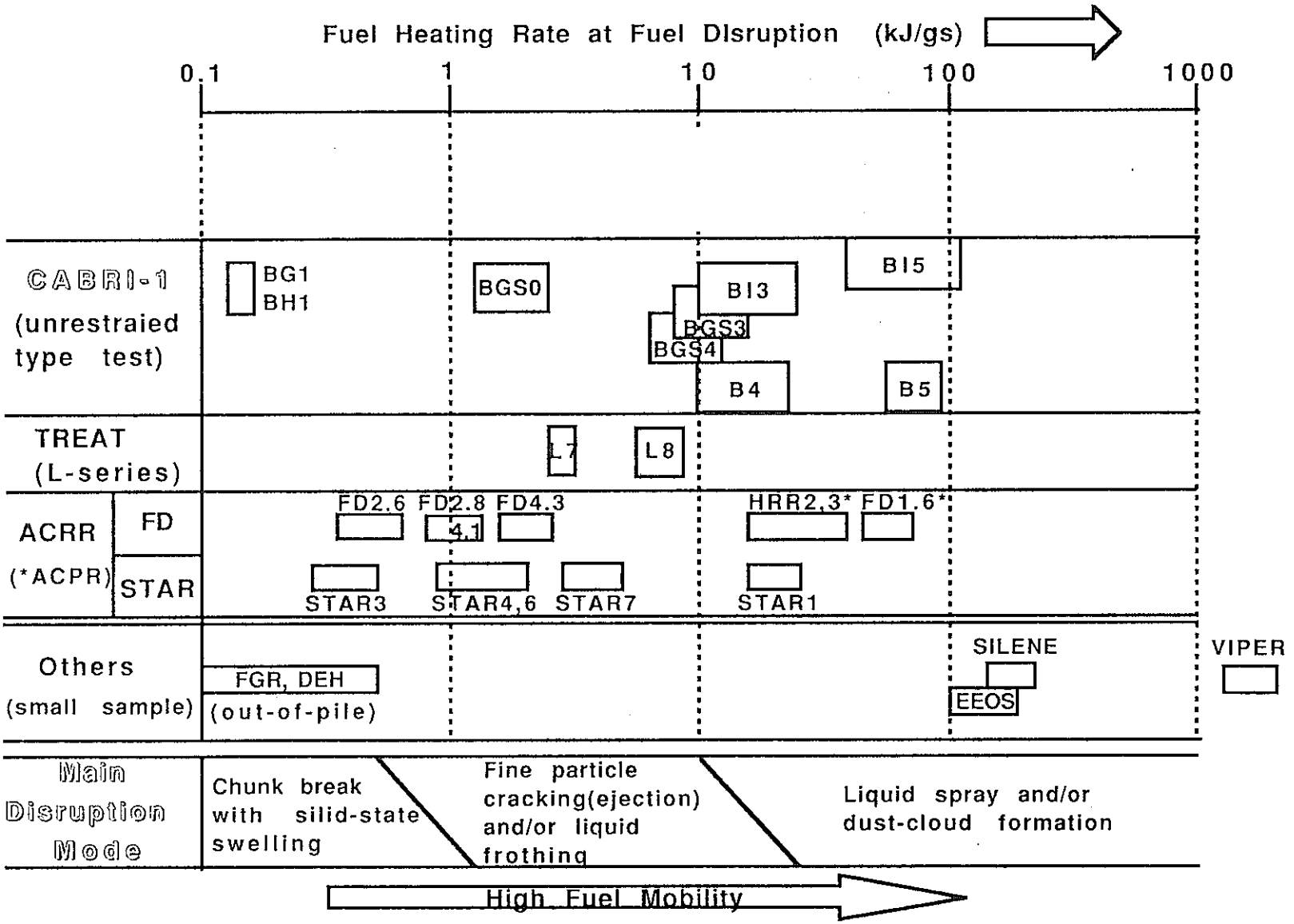

Fig. 8. FUEL HEATING-RATE RANGES IN FUEL DISRUPTION TESTS AND MAIN DISRUPTION MODES.

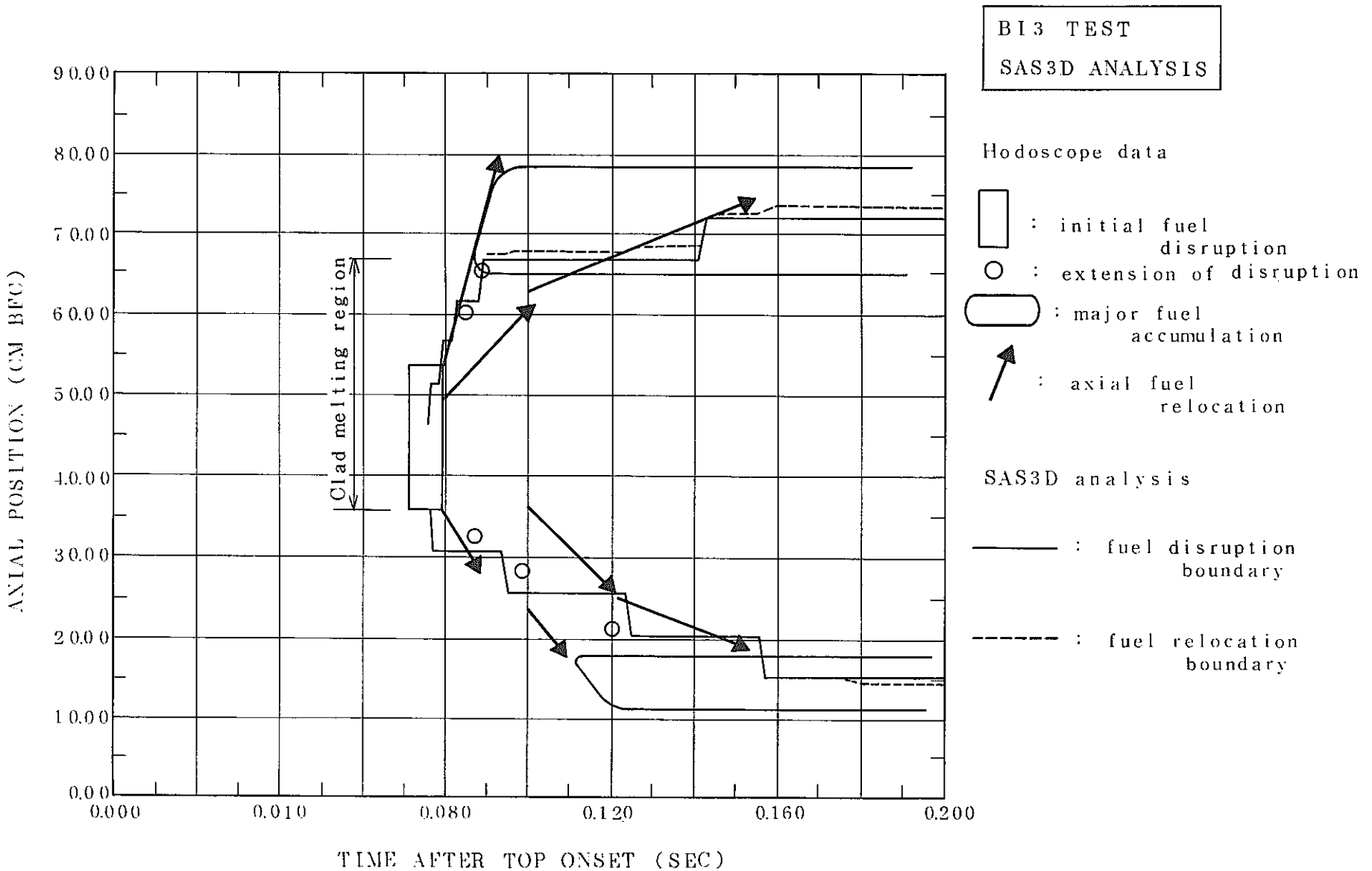

Fig. 9. Comparison of Fuel Disruption Boundaries between Experiment and SAS3D Analysis in CABRI BI3 Test.

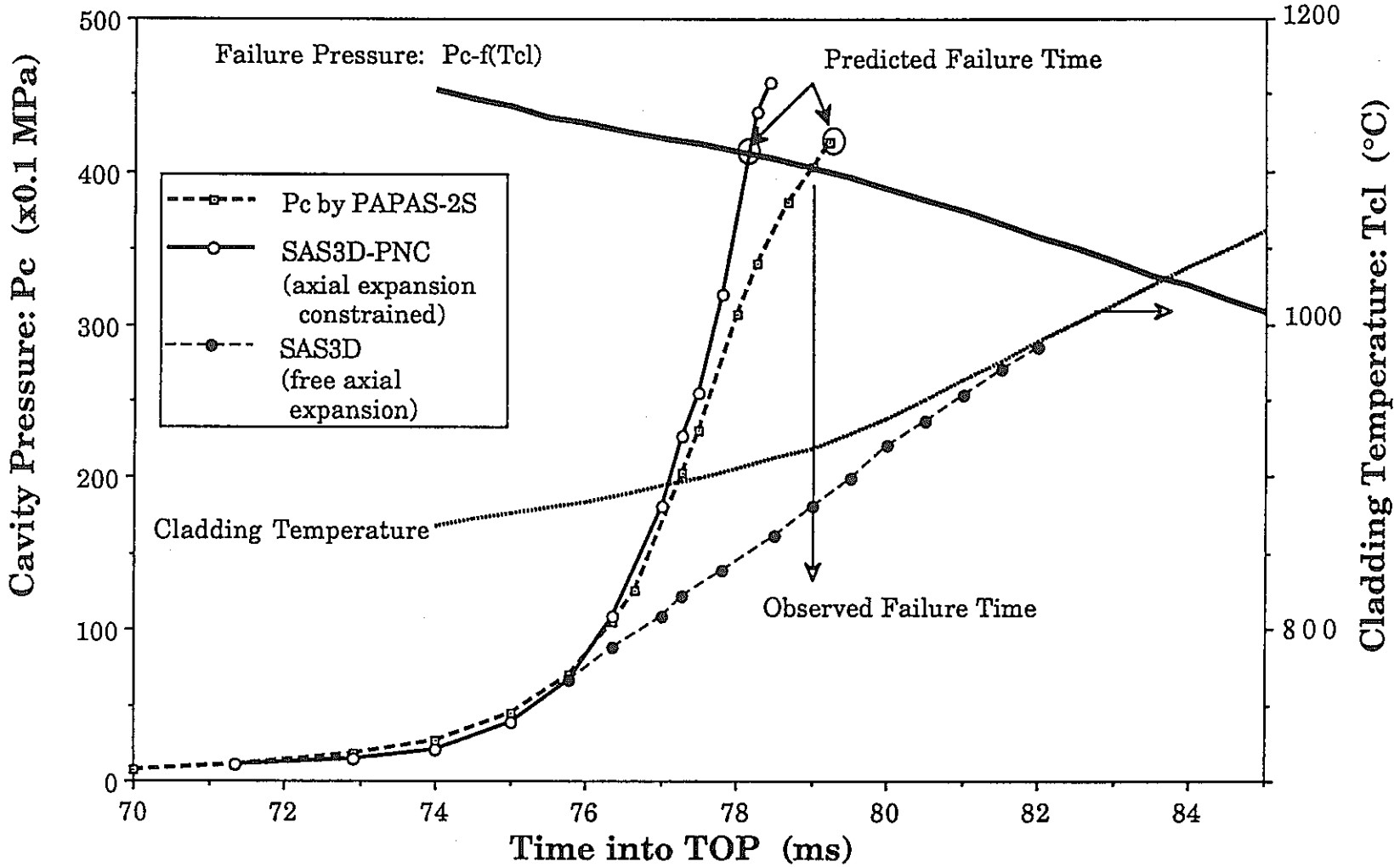

Fig. 10. Cavity Pressure Development and Failure Prediction in CABRI BI2 Test.

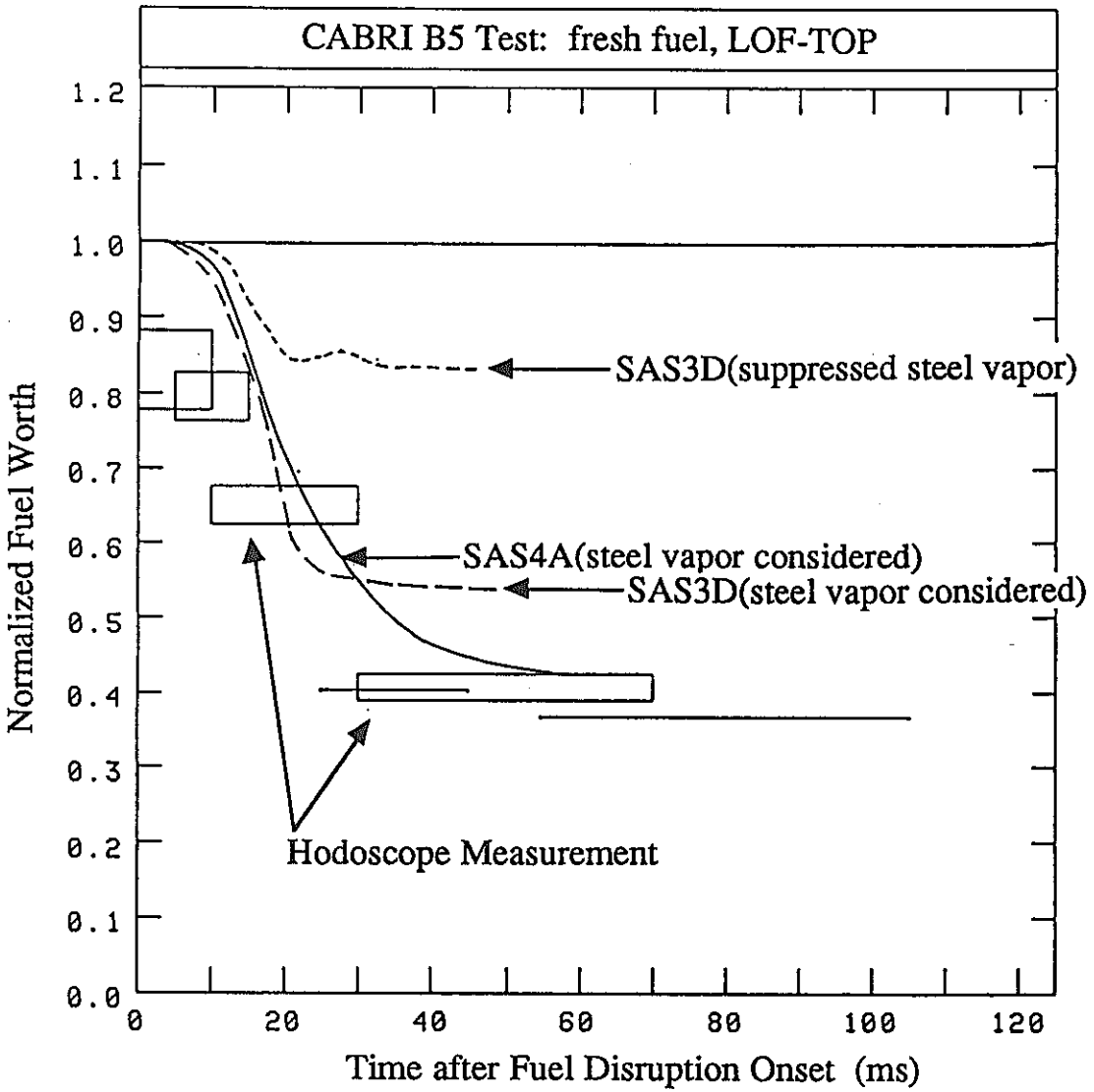

Fig. 11. Histories of Fuel Worth Change in Fuel Motion Analyses of CABRI B5 Test.

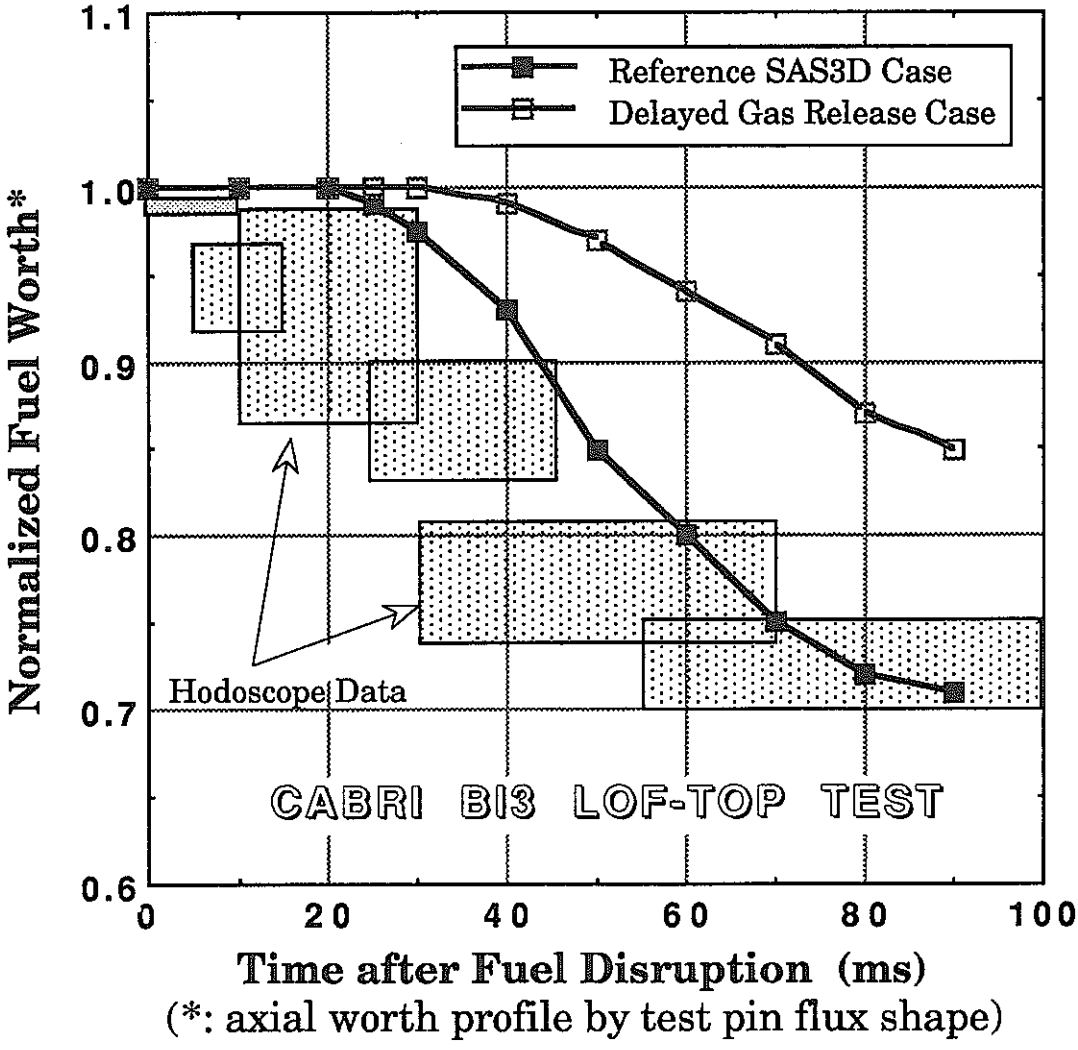

Fig. 12. Comparison of Fuel Worth Changes between Experiment and Analyses for BI3 Test.

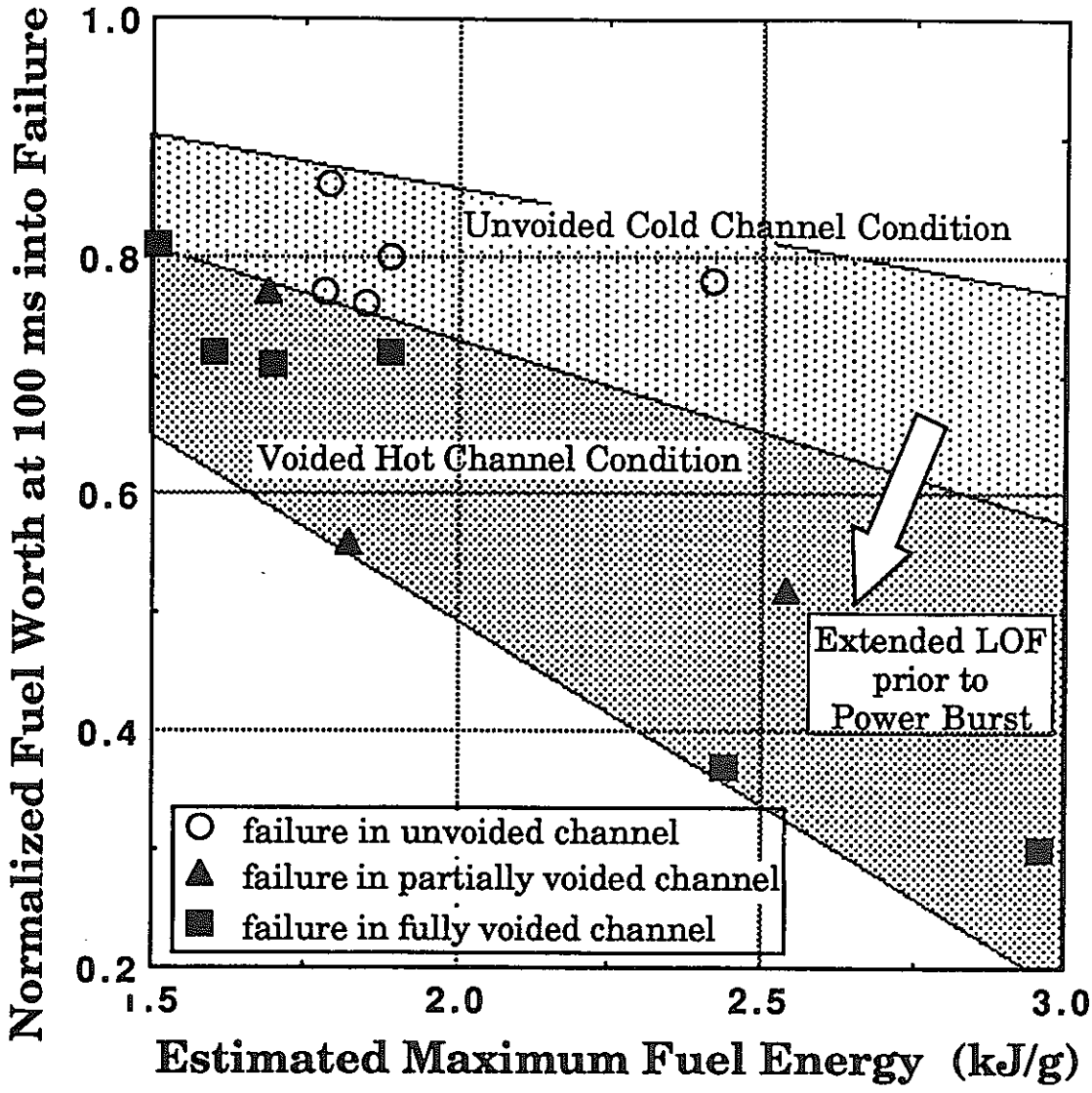

Fig. 13. Fuel Dispersal after Dynamic Fuel Relocation Phase in Different Energy and Cooling Conditions.

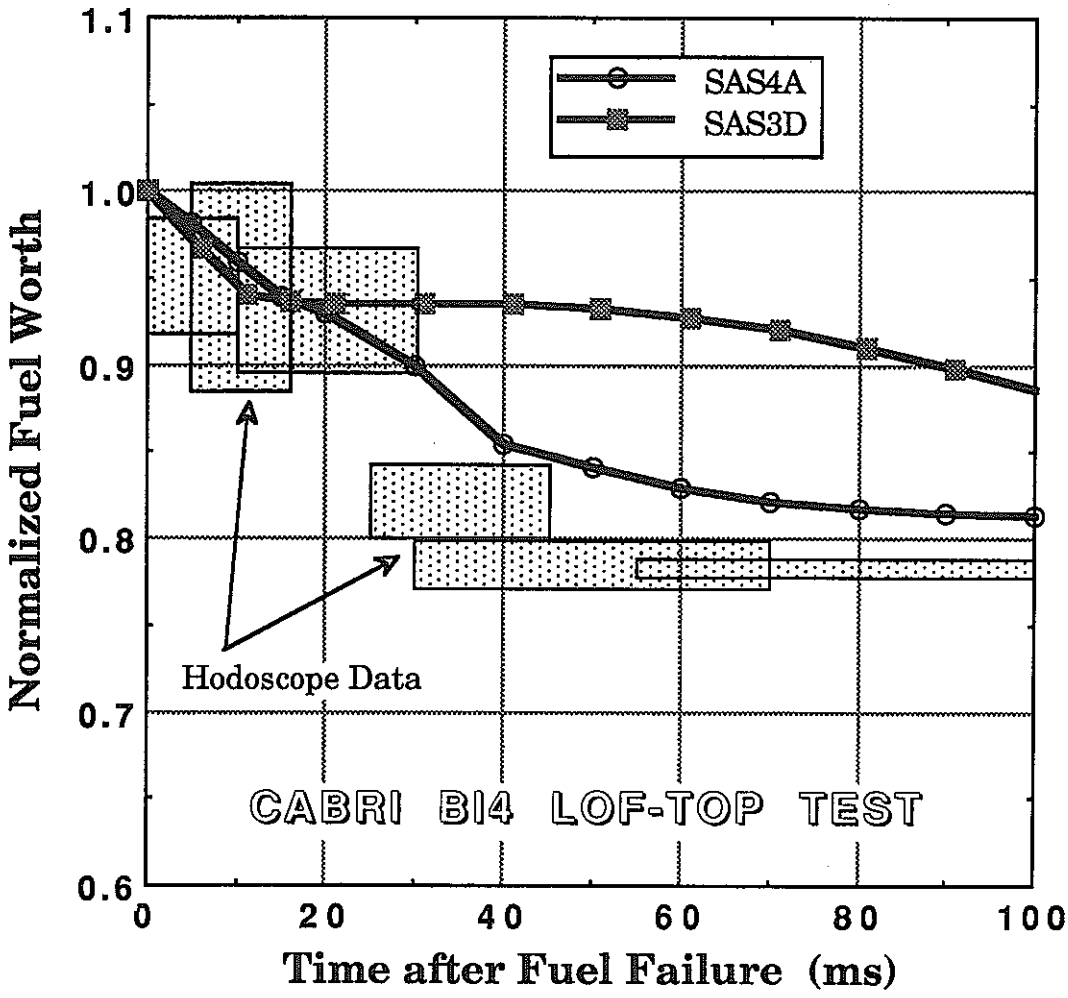

Fig. 14. Comparison of Fuel Worth Changes between Experiment and Analyses for BI4 Test.

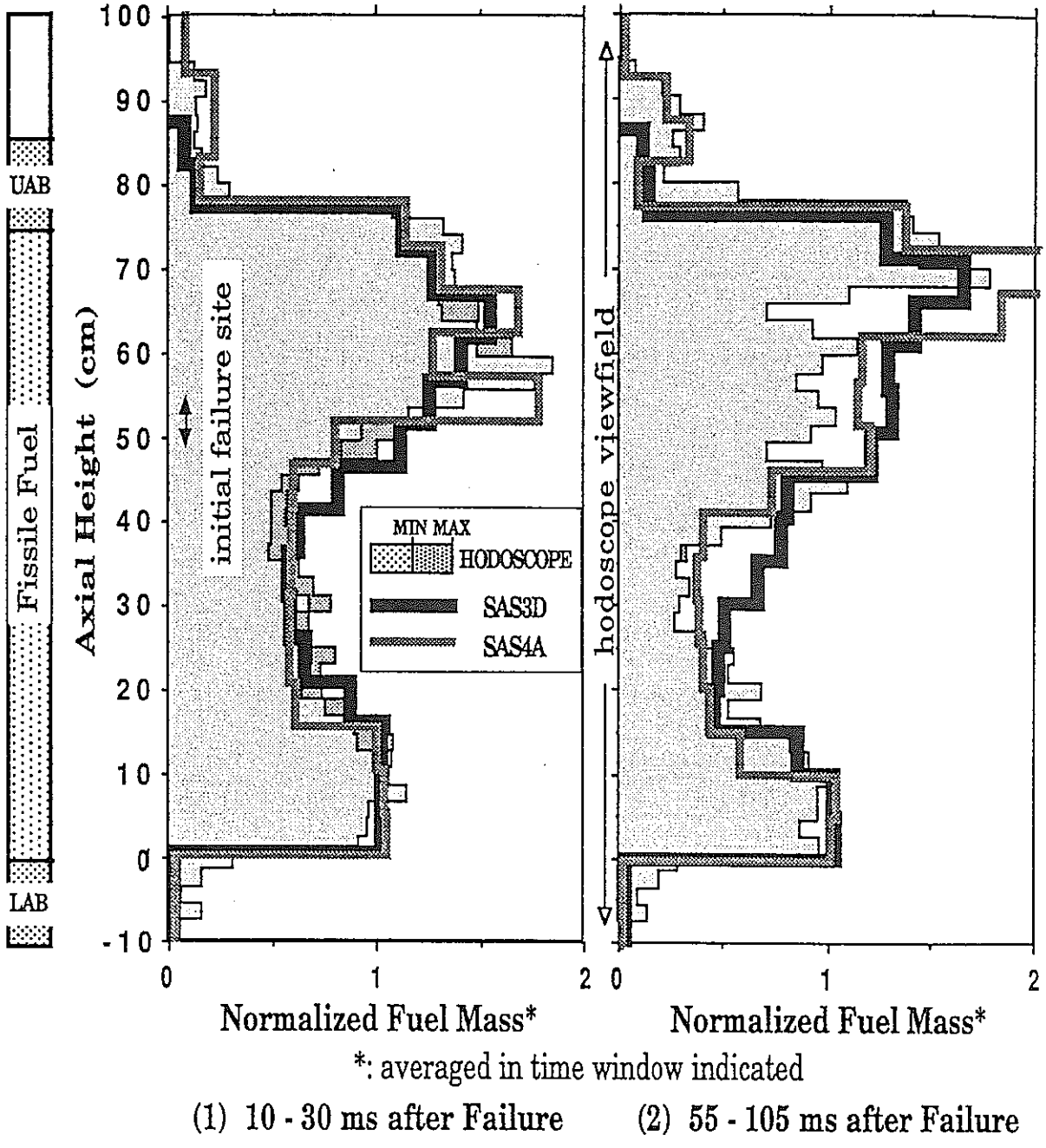

Fig. 15. Axial Fuel Distribution by hodoscope measurement and SAS3D/SAS4A analyses for BI4 Test.

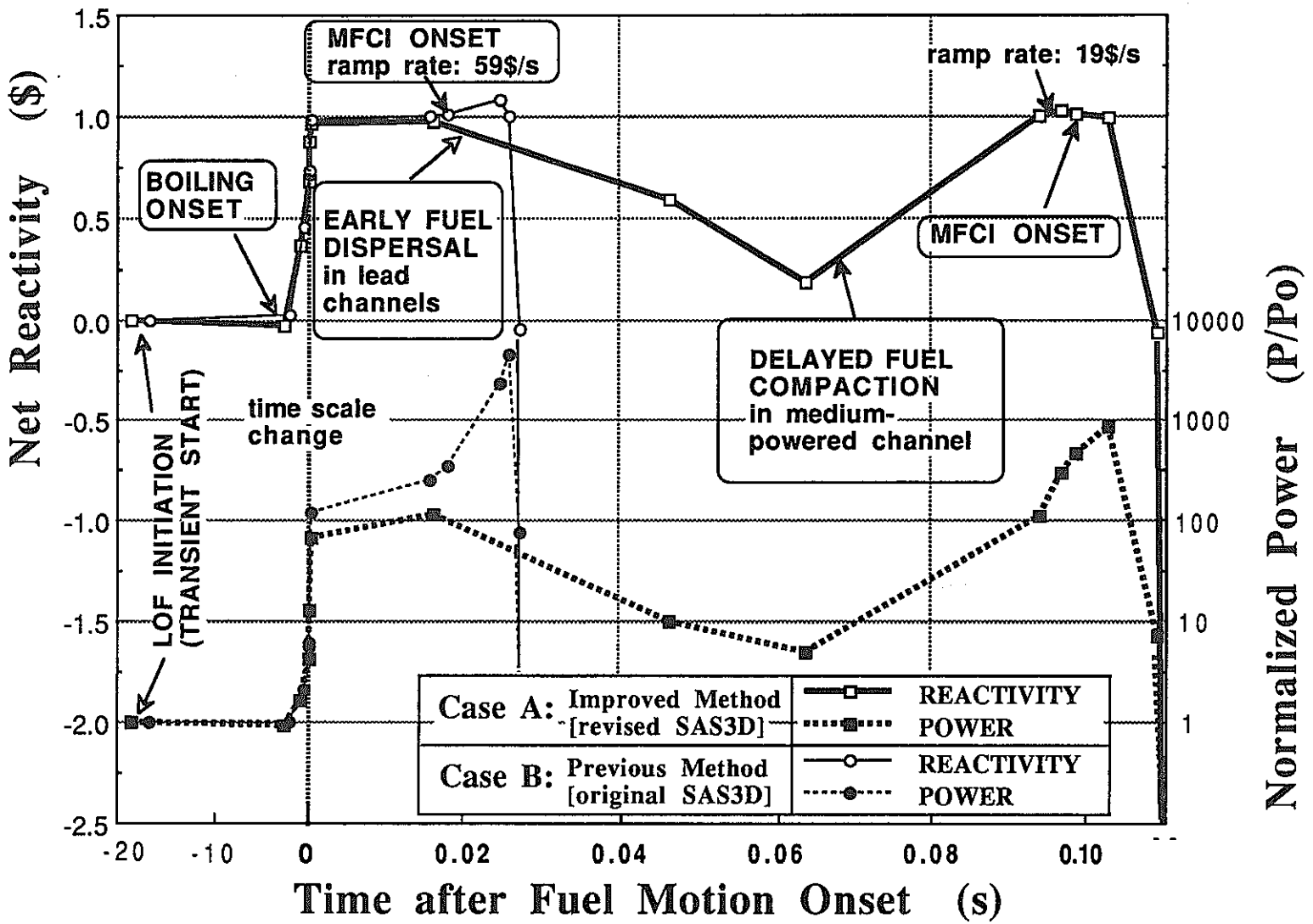

Fig. 16. Comparison of Reactivity and Power Traces for ULOF Analyses.
(New and Old Evaluation Methods)

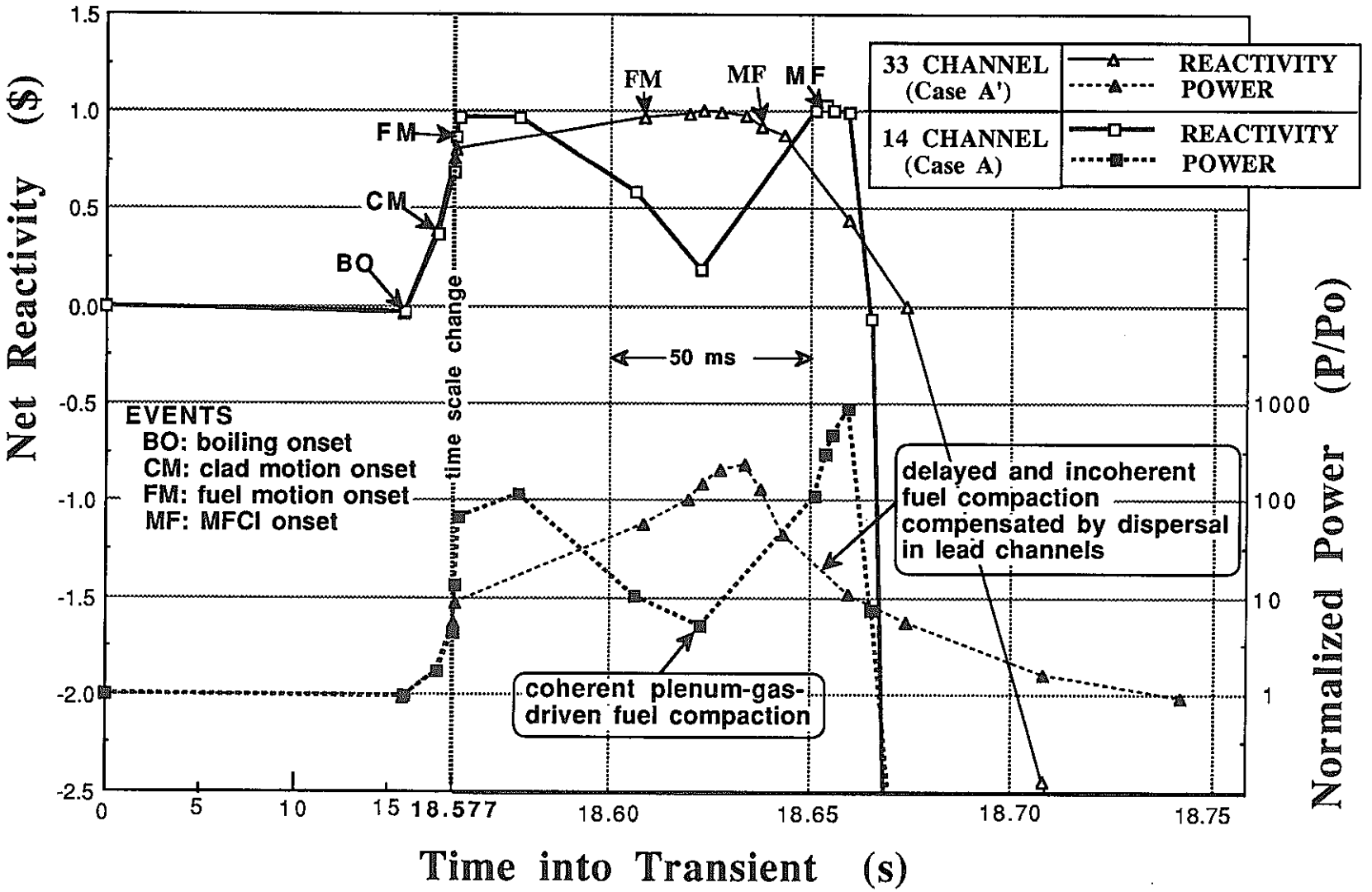

Fig. 17. Comparison of Reactivity and Power Traces between 33- and 14-Channel Analyses with Revised SAS3D Code.